Torque and Workspace Analysis for Flexible Tendon Driven Mechanisms

Maxime Chalon, Thomas Wimböck, Gerd Hirzinger

Institute of Robotics and Mechatronics, German Aerospace Center (DLR), Wessling, Germany

E-mails: {Maxime.Chalon, Thomas.Wimboeck}@dlr.de

Abstract— **Tendon driven mechanisms have been considered in robotic design for several decades. They provide lightweight end effectors with high dynamics. Using remote actuators it is possible to free more space for mechanics or electronics. Nevertheless, lightweight mechanism are fragile and unfortunately their control software can not protect them during the very first instant of an impact. Compliant mechanisms address this issue, providing a mechanical low pass filter, increasing the time available before the controller reacts. Using adjustable stiffness elements and an antagonistic architecture, the joint stiffness can be adjusted by variation of the tendon pre-tension. In this paper, the fundamental equations of m antagonistic tendon driven mechanisms are reviewed. Due to limited tendon forces the maximum torque and the maximum acheivable stiffness are dependent. This implies, that not only the torque workspace, or the stiffness workspace must be considered but also their interactions. Since the results are of high dimensionality, quality measures are necessary to provide a synthetic view. Two quality measures, similar to those used in grasp planning, are presented. They both provide the designer with a more precise insight into the mechanism.**

I. INTRODUCTION

Numerous new robot designs are based on tendon driven systems, for instance one finger of the integrated hand arm system of DLR is presented in Fig. 1. The advantages of tendon mechanisms are mainly low link inertia, remote actuation and high dynamics. Several research papers present the analysis of the workspace of parallel manipulators (such as [1]). Optimization methods, like convex techniques, have been applied to optimize the workspace [2]. But, the analyses are limited to the kinematic workspace and did not consider the use of variable stiffness mechanisms. The force limitation of the actuators creates constraints on the achievable torque and joint stiffness. Therefore, their interactions should be analyzed to understand the mechanism behavior.

In [3] Albu-Schäffer highlights that the intrinsic compliance, respectively the tendon pre-tension of robots, seen as a drawback in the past, can be a feature today. It is especially interesting in terms of protecting the robot itself. Indeed, since a control law can not react in the very first instant of the impact, the only protection of the robot is its intrinsic compliance [3].

Different mechanisms to adjust stiffness, for example the ANLES mechanism [4], have been studied with the help of stiffness ellipsoids (at the operating point). Stiffness and torque analysis of a variable stiffness joint, however, not considering tendons, can be found in [5]. A controller for

a variable stiffness mechanism using two motors and two springs in an antagonistic configuration is presented in [6].

Only little work is dealing with stiffness analysis of tendon driven systems with nonlinear tendon stiffness. Kobayashi [7] has investigated the question of serial tendon driven mechanisms with adjustable tendons stiffness. In such systems the joint torques are generated by rolling tendons around pulleys as shown in Fig. 2.
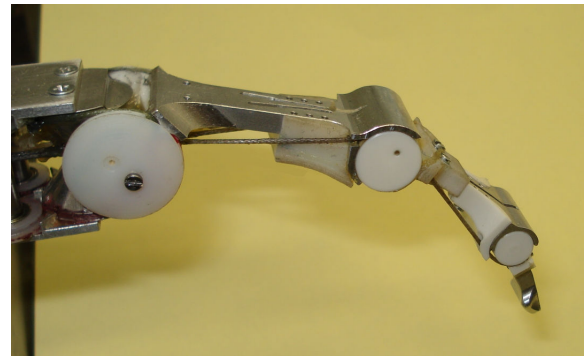

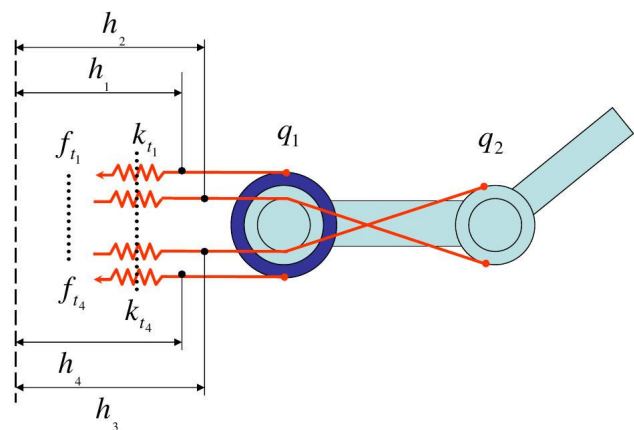Fig. 1. Single finger of the DLR Integrated Hand Arm System(4 DOF, 8 tendons)

Fig. 2. Two joints and their associated 4 tendons

The tendons are pulled by remote actuators. If flexible tendons are used in an antagonistic configuration, one part of the tendon forces generates joint torques and the other part, known as pretension, adjusts the intrinsic stiffness of

the joints. Examples of mechanisms used to obtain variable stiffness behavior can be found in [8]–[10]. At DLR a new integrated hand arm system, [11], is developed that combines a novel finger joint technology with variable stiffness elements. In Fig. 1 a prototype of one finger with four joints driven by eight tendons is presented.

The very specific configuration of mechansims with antagonistic flexible tendons creates new challenges. For such systems it is desirable to specify the position and the stiffness at the same time. However, if the actuation limits are taken into account the torque and stiffness ranges are not independent. Consequently, the output work must be restricted to some maximal load or be position dependent. The addition of a desired stiffness to the trajectory, by increasing the dimensionality, appeals for the use of new quality measures.

The main contribution of this paper is to extend the work of Kobayashi [7] by including actuator force limitations. The analysis of tendon driven mechanisms, as found in [4], [9], is extended by computing torque/stiffness workspace under actuator limitations. Several quality measures are introduced to evaluate if a given mechanism is suitable for a given task. The use of ratios is compulsory since the dimensionality of the results do not allow for simple 2D and 3D representation. In the first section, the fundamental equations that relate joint torques, tendon forces, tendon stiffness, and joint stiffness are established. The second section applies several quality measures to the analysis of variable stiffness elements that can help reducing the dimensionality of the results. The third section proposes an analysis tools for the sensitivity of the variable stiffness (VS) mechanism.

II. TORQUE/STIFFNESS MODELING

In this section, the derivation of two fundamental equations of tendon driven system with nonlinear tendon stiffness is presented. The notion of stiffness vector is introduced. It is shown that it takes a form that can be expressed in a simple way (under some conditions on the coupling matrix).

Table I defines the used symbols. The tendons are consid-

Symbol	Designation
$n \in \mathbb{N}$	number of mechanical degree of freedom (joints)
$m \in \mathbb{N}$	number of tendons
$h \in \mathbb{R}^m$	positions of the tendon w.r.t. a fixed reference
$q \in \mathbb{R}^n$	positions of the joint
$\tau \in \mathbb{R}^n$	joint torques generated by the tendon forces
$f \in \mathbb{R}^m$	forces applied on the tendon extremity
$K_t \in \mathbb{R}^{m \times m}$	stiffness matrix of the tendons
$K_q \in \mathbb{R}^{n \times n}$	stiffness matrix of the joints
$k_{t_i}(f_{t_i}) \in \mathbb{R}$	stiffness of the tendon depending on the tendon force
$P \in \mathbb{R}^{n \times m}$	coupling matrix

<div align="center">TABLE I</div>

<div align="center">DESCRIPTION OF VARIABLES</div>

ered to be fixed (as with non-backdrivable motors) and only static analysis is performed. More details about a dynamic analysis of such mechanisms can be found in [12]. The coupling matrix $P(q) \in \mathbb{R}^{n \times m}$, which relates the m tendon velocities $\dot{h} \in \mathbb{R}^m$ to the n joint velocities $\dot{q} \in \mathbb{R}^n$, is

obtained as the derivative of the tendon length h with respect to the joint position q.

$$P(q) = \left(\frac{\partial h(q)}{\partial q} \right)^T \qquad (1)$$

Using the principal of virtual work it yields:

$$\tau = P(q)f \qquad (2)$$

Because tendons can only pull, the number of tendons is greater than the number of joints for a fully actuated system [13]. The minimum number of tendon required for a fully actuated system is $n + 1$. Consequently, the coupling matrix is not square in general. It is assumed throughout this article that the coupling matrix has full row rank. If P has full rank, the system is said to be tendon *controllable* [7]. Using the previous definition of the coupling matrix the tendon forces can be decomposed in two parts,

$$f = P(q)^+ \tau + f_{int}$$

where P^+ is the generalized pseudo inverse and f_{int} is a force vector in the null space of $P(q)$. The pseudo inversion can be weighted such that the solution minimize a specific cost function [14]. Especially, the Moore-Penrose pseudo inverse minimizes the internal forces and distributes the forces equally (in the least mean squares sense). E.g., a weighting dependent on the actuator temperature could be used to avoid local overheating.

The tendon stiffness k_t is simply obtained as the derivative of the tendon force f with respect to the variation of the tendon length h (around the equilibrium point h_0),

$$k_t = \left. \frac{\partial f}{\partial h} \right|_{h=h_0}$$

Under the assumption that the tendons are not coupled directly, the tendon stiffness can be written in a diagonal matrix [1]:

$$K_t = diag\{k_{t_1}(f_1), ..., k_{t_m}(f_m)\} \qquad (3)$$

The tendon stiffness being a function of the tendon force it allows to obtain a variable joint stiffness by modulating the internal forces f_{int}. The dependency of the tendon stiffness upon the tendon force creates the capacity of adjusting the joint stiffness. The stiffness matrix of the joints, at an equilibrium point q_0 is defined as :

$$K_q(q_0) = \left. \frac{\partial \tau(q)}{\partial q} \right|_{q=q_0} \qquad (4)$$

Together with eq.(2) and assuming non-backdrivable motors [2]:

$$K_q = \frac{\partial P(q)}{\partial q} f(q) + P(q) \frac{\partial f(q)}{\partial q} \qquad (5)$$

---

[1] Throughout this paper $diag\{.\}$ applied to a matrix extracts its diagonal elements, applied to a vector it creates a matrix which diagonal elements are the vector elements

[2] Consideration on the control of system with back drivable motors are found in [12]

If the coupling matrix depends on the joint configuration, i.e. $\frac{\partial P}{\partial q} \neq 0$, it introduces another term that changes the joint stiffness. This results in a variable joint stiffness due to the variable transmission mechanism. Using eq.(1) and the definition of K_t in eq.(3) we obtain,

$$K_q(q) = \frac{\partial P(q)}{\partial q}f + P(q)K_tP(q)^T \qquad (6)$$

It can be shown that the joint stiffness matrix is always symmetric. Moreover, if the coupling is linear, i.e. $\frac{\partial P}{\partial q} = 0$, the joint stiffness matrix expression can be simplified. Thanks to the symmetry, only $n(n+1)/2$ coefficients are sufficient to describe the matrix K_q. There are n torques and $n(n+1)/2$ stiffness coefficients to control so intuitively $n(n+3)/2$ tendons are required [7]. In the case of mechanisms like fingers the full decoupling of all the coefficients is prohibitive in terms of tendons. For a 4 DOF finger 14 tendons would be needed, so 70 tendons for a 5 fingered hand. A trade-off has to be made and it is often chosen to use a $2n$ tendons configuration. In this case, the n torques and at most n stiffness coefficients are controllable. It is often decided to only control the diagonal terms and neglect the coupling terms. In the fingers of the DLR Hand Arm system, the tendon routing has been optimized in order to minimize the constraints due to the coupling. The vector of the joint stiffness can be advantageously rewritten as a linear combination of the tendon stiffness. To avoid repeating, in the following formulas, $i \in [1..n]$ and $j \in [1..m]$.:

$$s_q = diag(K_q) = S \, diag(K_t) \qquad$$

The form of the S matrix is easily obtained (if only the diagonal terms of the stiffness matrix are considered). The proof requires only few steps. $\delta(i,j)$ is the Kronecker symbol which is 1 if $i = j$ and 0 otherwise. The notation $M(i,j)$ is used to represent the element M_{ij}. First, the part $A = K_tP^T$ of the definition of K_q can be computed.

$$A(i,j) = \sum_{b=1}^{m} K_t(i,b)P^T(b,j) \qquad$$

Then the A matrix can be introduced again in the equation (6), looking carefully at the indices.

$$K_q(i,j) = \sum_{a=1}^{m} P(i,a)) \sum_{b=1}^{m} (K_t(a,b)P^T(b,j)) \qquad$$

Futhermore, given the diagonal shape of K_t the previous equation can be dramatically simplified.

$$K_q(i,j) = \sum_{a=1}^{m} P(i,a)) \sum_{b=1}^{m} (\delta(a,a)K_t(a,a)P^T(a,j)) \qquad$$

The second sum symbol can be dropped and the scalar reordered :

$$K_q(i,j) = \sum_{a=1}^{m} P(i,a))P^T(a,j)K_t(a,a) \qquad$$

Looking only at the diagonal coefficients, it follows

$$K_q(i,i) = \sum_{a=1}^{m} P(i,a))P^T(a,i)K_t(a,a). \qquad$$

This proves that the joint stiffness vector s_q can be written as

$$s_q = S \, diag(K_t), \qquad$$

where

$$S(i,j) = P(i,j)^2 \qquad$$

Using the two fundamental equations:

$$\begin{cases} \tau & = & Pf \\ s_q & = & diag(PK_t(f_t)P^T) \end{cases} \qquad (7)$$

It is possible to construct the mapping Ψ from the tendon force space Θ to the torque/stiffness workspace Ω. As:

$$\Psi: \quad \begin{matrix} \Theta \in [f_{min}..f_{max}]^m & \mapsto & \Omega \subset \mathbb{R}^m \\ f & \to & \begin{bmatrix} Pf \\ diag(P^TK_t(f_t)P) \end{bmatrix} \end{matrix} \qquad (8)$$

III. Analysis of the Torque/Stiffness workspace

The dimension of the workspace constructed in the previous section is usually too large to be displayed using conventional methods. However, in order to compare designs the dimensions must be reduced to offer interpretable information. Intuitive methods based on the minimum, maximum torque and stiffness, with which several indices are constructed, provide limited information. Although sufficient in the case of rigid mechanisms, they appear to be too limited in the case of stiffness adjustable mechanisms. Indeed, they do not capture the behavior of the elastic element and simulations/experiments have shown that the system performances vary largely upon the progression of the stiffness elements. Other types of analysis are also possible, for example an analysis that provide stiffness adjustable mechanisms classification can be found in [15]

A. Safety margin

A simple example is proposed to illustrate the possible limitations. Figure 3 shows two workspaces of a 1 DOF joint. The tendon maximum forces and the coupling matrix are identical. Only the stiffness characteristics have been changed.

$$\begin{matrix} A(f) & : & f^2 \\ B(f) & : & e^{\beta f} - \alpha, \; \beta = \frac{ln(A(f_{max})+\alpha)}{f_{max}} \end{matrix}$$

With $f \in [0, f_{max}]$, $P = [0.005, -0.005]$. It is easy to see that indices based on the extremes would not capture the differences.

To avoid this problem, it is proposed to introduce the notion of *safety margin*. The *safety margin* is defined as the radius of the biggest sphere that can be included in the workspace, as it can be done for grasp quality measure [16]. The sphere center C is either free or specified. If it is free the center of the optimal sphere can be interpreted as the natural
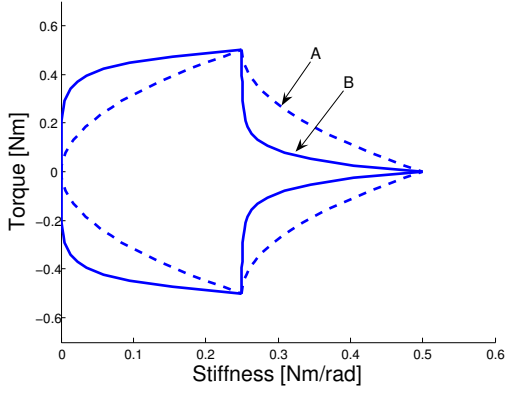
Fig. 3. Example where the min/max of the stiffness is not capturing the mechanim differences

working point of the mechanism and is called the *intrinsic safety center*, $\xi_{intrinsic}$. It is associated to its *intrinsic safety radius* (cf. Fig. 4 dotted circle).

If the center is specified, the sphere will give the distance to the mechanism limits for the specified working point. It is called *local safety center*, ξ_{local}. It is associated to its *local safety radius* (cf. Fig. 4 continuous circle). The local safety margin represents how well the mechanism perform given a task specification. The intrinsic margin gives the possibility of the robots. Using both margin th designer can iteratively adapt the mechanism to best fit his needs. The spheres are defined as :

$$\xi_{local}(C) = \max_{r \in \mathbb{R}}(B(C,r)|B \subset W) \qquad (9)$$

$$\xi_{intrinsic} = \max_{C \in \Omega}(\xi_{local}(C)) \qquad (10)$$

Where $B(C,r)$ is a ball of center C and radius r. W is the torque/stiffness workspace of the mechanism. The algorithm used to derived those measures performs gradient searches. It finds the minimum distance between the local center C and the workspace boundaries, i.e, when at least one tendon has reached its force limit. Indeed, a boundary point neccessarily belongs to a hypersurface of dimension $n - 1$, where one of the tendon is about to break ($f = f_{max}$). Applying this to each tendon leads to (m) surfaces from which a minimum distance to a point must be searched for. The gradient searches are smooth and do not pose any particular problems of convergence.

A random starting center, to avoid local minimum, and gradient search have been used to find the intrisinc center.

It must be noted that the complexity of the algorithms is growing with a factor m. It means that although efficient the nonlinear multipoint search can not garantee a global optimum.

The ratio of the intrinsic safety margin and the local safety margin is called the safety margin coverage and represents how well the mechanism is used compared to its natural abilities. It is a dimensionless value that can be used to compare, for example, different actuation principles. It must be noted that the radii have mixed units and certainly a weighting matrix is required to normalize the units (stiffness and torque). However, an algorithm to obtain such a weighting matrix is strongly task dependent (cf. the diversity of weighting matrix found in manipulability analysis). The designer has the task (and the knowledge) to decide the relative importance of stiffness versus torque. Similarly, he can decide to give more importance to a specific joint. The understanding of the task is necessary to create the appropriate weighting. For a 1 DOF joint it is possible to see the results but in higher dimension only an appropriate weigting can garantee a correct result.

The following design problem aims at improving a single joint mechanism that is operated around a given working point $\omega = (0.2Nm, 0.25Nm/rad)$

The initial design uses two identical tendon with the characteristics:

f_{max} [N]	100
k [N/m]	f^2
P [m]	$[0.005, -0.005]$

TABLE II

TENDON CHARACTERISTICS

A modified design, with the manually improved coupling matrix, $P = [0.0063, -0.0037]$, is proposed. The original and modified workspaces are shown in the figure 4 and 5[3], the results of the ratios are reported in the table III.
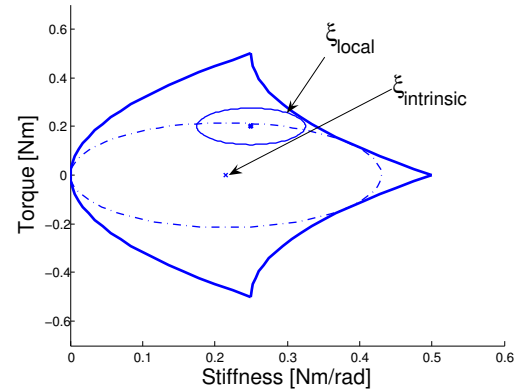

Fig. 4. Original coupling, the dotted circle is the intrinsic safety, the continuous circle is the local safety

Although the intrinsic radius of the mechanism has been reduced, the coupling is more adapted to the working point. It can be seen that the local safety radius is larger. The best solution for this problem, and given this ratio, is naturally to adjust the coupling matrix such that the intrinsic center and the desired working point are identical.

The previous analysis can be scaled to higher dimensions without modifications. It enables the designer to compare

---

[3]The circles only appear as ellipsoids because of the graph scales. The calculations are performed without any weighting matrix.
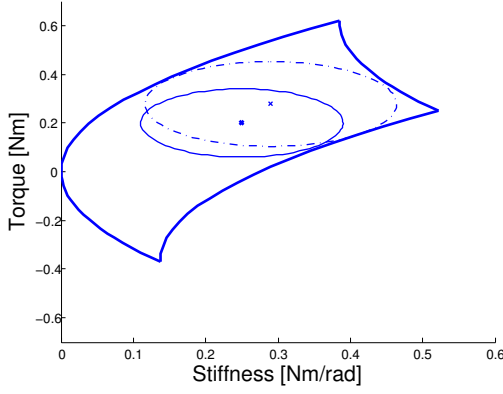
Fig. 5. Improved Coupling, the dotted circle is the intrinsic safety, the continuous circle is the local safety

		center	radius	quality measure
before	intrinsic	[0.215, 0]	0.215	
	local	[0.25,0.2]	0.075	0.12
after	intrinsic	[0.278, 0.290]	0.174	
	local center	[0.25,0.2]	0.14	0.64

mechanisms very easily when he is targeting a specific working point. If the design is unsatisfactory, he can select a different stiffness curve of the mechanism, or modify the coupling. This approach has been used at DLR to select the stiffness elements that will be used in the wrist of the DLR Hand Arm System [11].

B. Sensitivity

The use of non linear stiffness elements means that the stiffness and the torque can be adjusted, but it is important to know how well they can be selected. If the input is sampled uniformly, the output points distribution gives the image of the sensitivity. To obtain a synthetic value from the distribution, several statistics tools are available. However, it has been decided to only use the first moment of the data, because the interpretation of the results is difficult in high dimensions. The first moment is also known as the center of gravity. It is proposed to use a ratio λ between the first moment of the output space, $G(\Omega)$, and the image of the first moment of the input space, $\Psi(G(\Theta))$. Namely,

$$\lambda = \frac{\min(\|G(\Psi(\Theta))\|, \|\Psi(G(\Theta))\|)}{\max(\|G(\Psi(\Theta))\|, \|\Psi(G(\Theta))\|)},$$

where Ψ is the mapping application, $\Theta = [0..f_{max}]^m$ and G gives the first moment of a set. The following figure represents the mapping Ψ from $\Theta = [0..100N]^2$ to Ω. The transformation of the center of gravity of the force space $G(\Theta)$ to the troque/stiffness workspace Ω is shown with an arrow (cf. Fig. 6). The coordinates of $G(\Theta)$ represent the center of the achievable actuation forces. Its image by Ψ, represents the torque and stiffness obtained when all
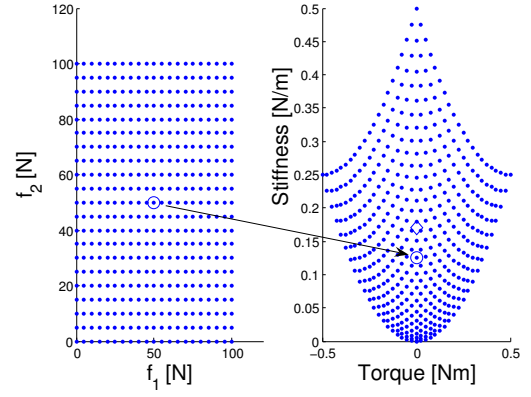

Fig. 6. Representation of the mapping from the force space Θ to the torque/stiffness workpsace Ω. The arrow indicates the tranformation of the center of gravity ($\Psi(G(\Theta))$)

actuators are at the center of their force workspace. The set $\Psi(\Theta)$ is the set of torques and stiffness values that the mechanism can achieve. The principal idea is that the distortion of this space gives a good idea of the systems nonlinearities. However, since a simple figure is wanted, the metric concentrate only on the distortion that occurs on the center of gravity (one could also use several points, or the surface change of a simple geometry figure).

The definition can be applied to a system of any dimension. However, to be able to compare the results to a graphic, an example in 1D is presented. The values used are summarized in table IV.

f_{max} [N]	100
k_1 [N/m]	f^2
k_2 [N/m]	$e^{\beta f} - 1, \beta = \frac{ln(k_1(f_{max})+1)}{f_{max}}$
P_1 [m]	[0.005, −0.005]
P_2 [m]	[0.0062, −0.0037]
Θ	$[0..f_{max}]^m$

The figures 7, 8 and 9 show the output set Ω (i.e. torque and stiffness of the joint), obtained as $\Psi(\Theta)$, for different choices of P_i and k_i.

The table V, presents the results.

Coupling	Stiffness function	λ
P_1	k_1	0.833
P_1	k_2	0.082
P_2	k_1	0.902

In those simple cases it appears clearly that the stiffness function k_2 is compressing the workspace around the origin and leads to a very poor sensitivity in the remaining space. The stiffness function k_1 is spreading uniformly the values
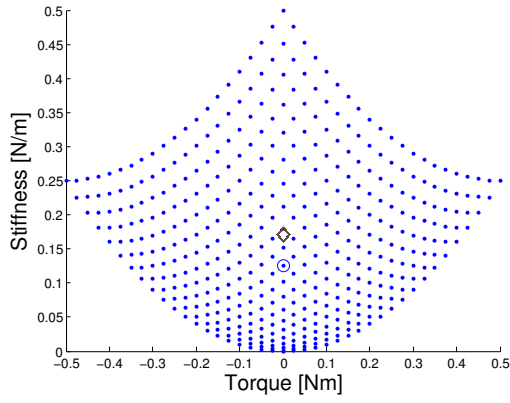
Fig. 7. The diamond is $G(\Psi(\Omega))$, the circle $\Psi(G(\Omega))$ with P_1 and k_1
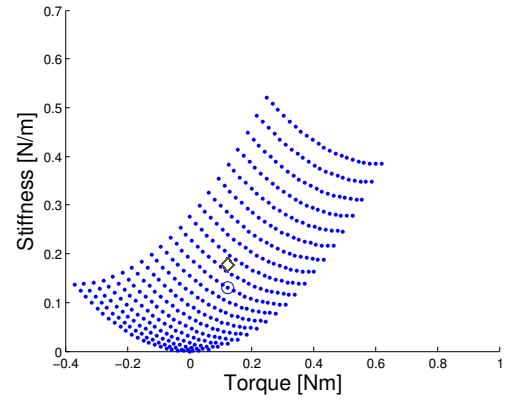

Fig. 9. The diamond is $G(\Psi(\Omega))$, the circle $\Psi(G(\Omega))$ with P_2 and k_1
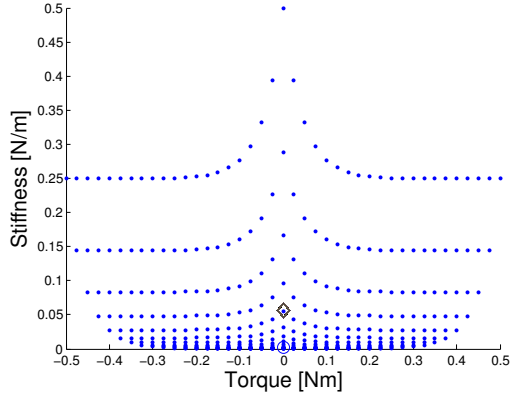

Fig. 8. The diamond is $G(\Psi(\Omega))$, the circle $\Psi(G(\Omega))$ with P_1 and k_2

f_{max} [N]	100
k_1 [N/m]	f^2
k_2 [N/m]	$e^{\beta f} - 1, \beta = \frac{ln(k_1(f_{max})+1)}{f_{max}}$
P_1 [m]	$\begin{bmatrix} 0.005 & 0 \\ 0.005 & -0.002 \\ -0.005 & 0.002 \\ -0.005 & 0 \end{bmatrix}$
P_2 [m]	$\begin{bmatrix} 0.005 & 0 \\ 0.002 & -0.002 \\ -0.004 & 0.001 \\ -0.005 & 0 \end{bmatrix}$
Θ	$[0..f_{max}]^m$

TABLE VI

PARAMTERS USED FOR THE 2D SENSITIVITY EXAMPLE

Coupling	Stiffness function	λ
P_1	k_1	0.03
P_1	k_2	0.714
P_2	k_1	0.771

TABLE VII

RESULTS OF THE RATIO ON THE DIFFERENT 2D SENSITIVITY EXAMPLES

and thus the ratio is really close to one. As mentioned earlier, the ratio can be used in higher dimension but, of course, for the graphical representation appropriate projections are needed. The table VI is presenting the data used for a 2D analysis of the stiffness curve on the sensitivity ratio. Table VII reports the sensitivity ratio results. As expected, the results obtained with the exponential stiffness function are very low compared to the quadratic stiffness function. This is due to the contraction of the exponential function near the origin. Since they are linear, the coupling matrices P_1 or P_2 have little influence on the sensitivity. They do not really modifiy the distribution of Ψ. The effect of the coupling would however be visible when using the safety margin quality measure.

IV. CONCLUSION AND FUTURE WORK

The derivation of the joint stiffness matrix has been presented. Under some commonly respected condition, the torque and stiffness equations can be put together to obtain a synthetic description of the system. In particular it has been shown that in case of symmetric coupling the "joint stiffness vector" s_q can be computed very efficiently.

But, as pointed out in [17], the interpretation of results in more than three dimensions requires the use of a quality measures. Two new quality measures have been proposed,

the safety margin concept and the sensitivity concept. They both apply to high dimensional spaces, although their calculation require some specialized algorithms. The safety margin concept provides a synthetic measure of the capabilities of the mechanism. Contrary to previous quality measures, it captures the stiffness behaviour, hence allowing to select the proper stiffness elements. An example has been proposed to show how the safety margin can be used to improve the coupling matrix of a single joint.

A second quality measure, based on the mapping density, is used to measure the capabilities to adjust the stiffness or torque. Those two new tools are used in the context of several hand development at the DLR robotic institute.

The undergoing research concentrates on the development of an efficient method to solve the system torque/stiffness equations. Methods to efficiently compute the quality measures in high dimension is also under investigation.

REFERENCES

[1] M. M. Aref and H. D. Taghirad, "Geometrical workspace analysis of a cable-driven redundant parallel manipulator: KNTU CDRPM," *IEEE/RSJ International Conference on Intelligent Robots and Systems Acropolis Convention Center*, 2008.

[2] M. Hassan and A. Khajepour, "Optimization of actuator forces in cable-based parallel manipulators using convex analysis," *IEEE Transactions on Robotics*, vol. 24, no. 3, pp. 736–740, 2008.

[3] A. Albu-Schäffer, O. Eiberger, M. Grebenstein, S. Haddadin, C. Ott, T. Wimböck, S. Wolf, and G. Hirzinger, "Soft robotics: From torque feedback controlled lightweight robots to intrinsically compliant systems," *IEEE Robotics and Automation Magazine*, vol. 15, no. 3, pp. 20–30, 2008.

[4] K. Koganezawa, T. Nakazawa, and T. Inaba, "Antagonistic control of multi-dof joint by using the actuator with non-linear elasticity," 2006, pp. 2201–2207.

[5] S. Wolf and G. Hirzinger, "A new variable stiffness design: Matching requirements of the next robot generation," *2008 IEEE International Conference on Robotics and Automation*, 2008.

[6] R. Schiavi, G. Grioli, S. Sen, and A. Bicchi, "VSA-II: A novel prototype of variable stiffness actuator for safe and performing robots interacting with humans," in *IEEE International Conference on Robotics and Automation*, 2008, pp. 2171–2176.

[7] H. Kobayashi, K. Hyodo, and D. Ogane, "On tendon-driven robotic mechanisms with redundant tendons," *International Journal of Robotics Research*, vol. 17, no. 5, pp. 561–571, 1998.

[8] F. Laurin-Kovitz, K. Colgate, J. Carnes, and D. Steven, "Design of components for programmable passive impedance," *Proceedings - IEEE International Conference on Robotics and Automation*, vol. 2, pp. 1476–1481, 1991.

[9] K. Koganezawa and M. Yamazaki, "Mechanical stiffness control of tendon-driven joints," in *Proceedings of the IEEE/RSJ International Conference on Intelligent Robots and Systems*, vol. 3, 2002, pp. 2280–2285.

[10] H. Kino, N. Okamura, and S. Yabe, "Basic characteristics of tendon-driven manipulator using belt pulleys," in *Proceedings of 2004 IEEE International Conference on Intelligent Robots and Systems*, vol. 2, 2004, pp. 1287–1292.

[11] M. Grebenstein and P. van der Smagt, "Antagonism for a highly anthropomorphic hand arm system," *Advanced Robotics*, no. 22, pp. 39–55, 2008.

[12] T. Wimböck, C. Ott, A. Albu-Schäffer, A. Kugi, and G. Hirzinger, "Impedance control for variable stiffness mechanisms with nonlinear joint coupling," in *IEEE International Conference on Intelligent Robots and Systems*, 2008, pp. 3796–3803.

[13] M. W. Spong, S. Hutchinson, and M. Vidyasagar, *Robot Modeling and Control*. ISBN 81-265-0766-7, 2006.

[14] T. N. Greville, *Generalized Inverses*. Springer-Verlag, 2003.

[15] M. G.Catalano, R. Schiavi, and A. Bicchi, "Design of variable stiffness actuators mechanisms based on enumeration and analysis performance," in *ICRA*. IEEE, 2010.

[16] C. Borst, M. Fischer, and G. Hirzinger, "Grasp planning: How to choose a suitable task wrench space," *Proceedings - IEEE International Conference on Robotics and Automation*, vol. 2004, no. 1, pp. 319–325, 2004.

[17] K. Shimoga, "Robot grasp synthesis algorithms: A survey," *The International Journal of Robotics Research*, vol. 15, no. 3, pp. 230–266, 1996.